



ACADEMIC
PRESS

Available online at www.sciencedirect.com

SCIENCE @ DIRECT®

Journal of Solid State Chemistry 171 (2003) 152–160

JOURNAL OF
SOLID STATE
CHEMISTRY

<http://elsevier.com/locate/jssc>

Size and morphology control of Y_2O_3 nanopowders via a sol–gel route

A. Dupont,^{a,*} C. Parent,^a B. Le Garrec,^b and J.M. Heintz^a

^aICMCB-CNRS, Université Bordeaux 1, 87 Av. A. Schweitzer, 33608 Pessac Cedex, France

^bCEA/CESTA, 15 Av. des Sablières, BP no. 2, 33114 Le Barp, France

Received 22 May 2002; received in revised form 1 September 2002; accepted 17 November 2002

Abstract

The present paper deals with the preparation of nanometric yttria powders. A sol–gel method has been adopted to synthesize a precursor gel which, after being heated, leads to Y_2O_3 . Two main parameters are taken into account: the nature of the chelating agent and the [chelating agent]/[Y] relative concentration. The influence of these parameters on the composition and crystallization state of the precursor gel has been studied in the first part and on the grain morphologies of the resulting yttria powder in the second part. It has been shown that, depending on the chelating agent, nanometric powders presenting either needles, platelets or spherical shapes can actually be obtained at 800°C or 1100°C.

© 2003 Elsevier Science (USA). All rights reserved.

Keywords: Yttria; Sol–gel; Nanometric; Morphology; Topochemistry

1. Introduction

Preparation of ceramics as dense materials has given rise to many publications in recent years because of potential applications of such ceramics in the optical and opto-electronics fields. However, obtaining transparent ceramics requires a final density of 100% and thus a strict control of the characteristics of initial powders. Actually, densification ability highly depends on powder specificities like grain size, distribution size, grain morphology and grain agglomeration state. Chemical synthesis of the powders is probably the best way to control these characteristics and especially sol–gel type processing which is a powerful route to obtain ultra-fine particles with a controlled morphology.

Articles related to the preparation of fine powders for transparent ceramics have been reported in the literature, concerning mainly $Y_3Al_5O_{12}$ and in a lesser proportion Y_2O_3 . These methods included sol–gel processing, hydroxide co-precipitation, homogeneous precipitation, glyothermal treatment, spray pyrolysis, and combustion synthesis [1–5].

Our paper deals with yttria powder synthesis. Actually, previous works using either urea [6] or polyacrylic acid [7] have pointed out the role of the chelating media on the microstructural characteristics of the fine powders obtained. Therefore, a detailed study has been carried out to investigate the effect of the chelating agent on particle morphologies, even after high-temperature calcination treatment. Very large differences in size and shape were obtained depending on the nature of the organic acid used as chelating agent and on its concentration ratio relative to yttrium in the initial solution.

2. Experimental procedure

2.1. Synthesis

Yttria powders have been synthesized by the sol–gel route involving different chelating agents. Influence of their concentration on gel and powder characteristics has also been studied. Two different [chelating agent]/[Y] ratios were considered, i.e., 2 and 20. pH was initially adjusted to pH = 2 for all cases.

*Corresponding author. Fax: +33-(0)556-84-2761.

E-mail address: dupont@icmcb.u-bordeaux.fr (A. Dupont).

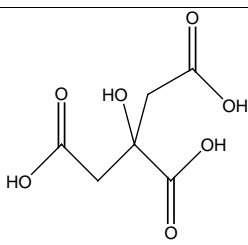
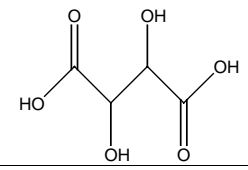
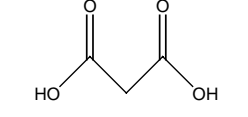
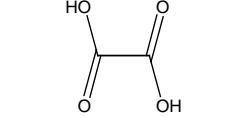
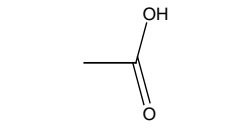
Name of chelating agent	Organic acid formula	Predominant form due to pH range				
Citric acid $C_6H_8O_7$		<p>↓ 3,13 4,76 6,4</p> <table border="1"> <tr> <td>H_3Cit</td> <td>H_2Cit^-</td> <td>$HCit^{2-}$</td> <td>Cit^{3-}</td> </tr> </table>	H_3Cit	H_2Cit^-	$HCit^{2-}$	Cit^{3-}
H_3Cit	H_2Cit^-	$HCit^{2-}$	Cit^{3-}			
DL-Tartaric acid $C_4H_6O_6$		<p>↓ 3,03 4,37</p> <table border="1"> <tr> <td>H_2Tar</td> <td>$HTar^-$</td> <td>Tar^{2-}</td> </tr> </table>	H_2Tar	$HTar^-$	Tar^{2-}	
H_2Tar	$HTar^-$	Tar^{2-}				
Malonic acid $C_3H_4O_4$		<p>↓ 2,85 5,7</p> <table border="1"> <tr> <td>H_2Mal</td> <td>$Hmal^-$</td> <td>Mal^{2-}</td> </tr> </table>	H_2Mal	$Hmal^-$	Mal^{2-}	
H_2Mal	$Hmal^-$	Mal^{2-}				
Oxalic acid $C_2H_2O_4$		<p>1,25 ↓ 3,81</p> <table border="1"> <tr> <td>H_2Ox</td> <td>Hox^-</td> <td>Ox^{2-}</td> </tr> </table>	H_2Ox	Hox^-	Ox^{2-}	
H_2Ox	Hox^-	Ox^{2-}				
Acetic acid $C_2H_4O_2$		<p>↓ 4,6</p> <table border="1"> <tr> <td>$AcOH$</td> <td>AcO^-</td> </tr> </table>	$AcOH$	AcO^-		
$AcOH$	AcO^-					

Fig. 1. Organic acids used as chelating agents and predominant forms due to pH range.

Fig. 1 presents the organic acids which were used, the associated formulae and the predominant form that can be expected based on the value of pH. All these reagents were reagent-grade quality (acetic acid, Aldrich 99.7%, oxalic acid, Alfa Aesar, 99.5%, malonic acid, Merck, 99%, tartaric acid, Aldrich, 99%, citric acid, Aldrich, 99%). Yttrium was introduced as yttrium nitrate hexahydrated (Alfa Aesar, 99.9%). It was dissolved in water so that yttrium concentration was 0.5 mol L^{-1} . Organic acid was then slowly added as aqueous solution until the chosen [chelating agent]/[Y] ratio was satisfied. pH was then adjusted to 2 with 30% ammonia solution (Carlo Erba, for analysis). The aqueous solution obtained was then heated at 115°C for 12 h and a gel formed. For oxalic and tartaric routes, owing to the low viscosity of the gel, a washing step (the gel was filtered and dispersed in distilled water four times) was added to remove impurities such as NO_3^- and NH_4^+ . For other chelating agents, gel stiffness prevented this washing step to be done. Whatever organic acid precursors were used, the resulting products were finally heat treated at 800°C or 1100°C , in a flowing

oxygen atmosphere with a heating rate of 200°C h^{-1} and a holding time of 4 h. Fig. 2 summarizes the experimental procedure.

In the particular cases of [malonic acid]/[Y]=2 and [acetic acid]/[Y]=20 ratios, an auto-combustion process was observed. In these cases, sample calcination was not performed in a furnace but on a hot plate. A self-propagating ignition process spread in a few seconds to the whole sample at about 270°C in the case of malonic acid and 340°C for acetic acid. This auto-combustion process suddenly released a large volume of gases and the gel swelled into an ultra-porous material, black in the case of malonic acid and white for acetic acid.

A blank gelification experiment was also performed in order to check rare-earth effect on the gelification process. Organic acid was dissolved in distilled water in the same amount as previously mentioned and ammonium nitrate was slowly added so that nitrate concentration was the same as in the first experiment with yttrium. pH was then adjusted to 2 with ammonia and this aqueous solution was heated for 15 h at 115°C .

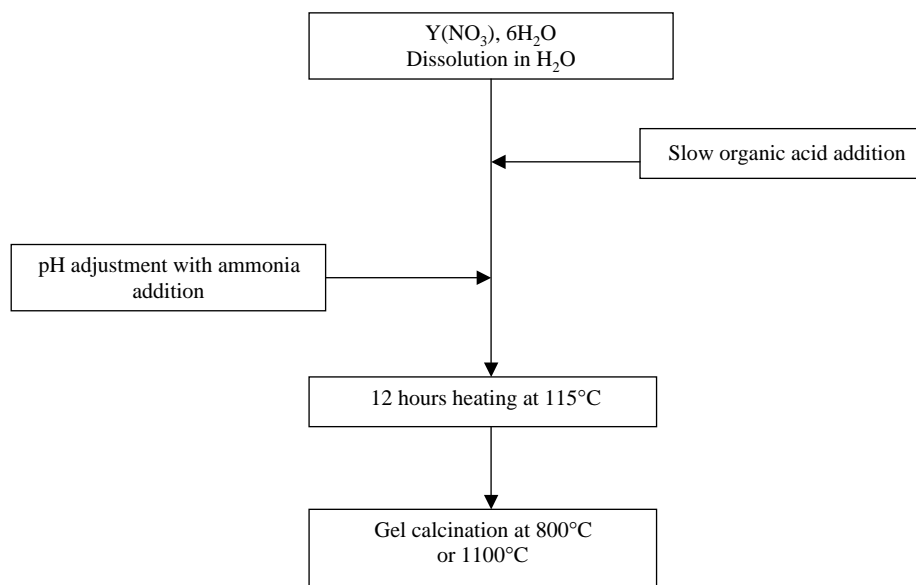


Fig. 2. Experimental procedure.

2.2. Experimental techniques

Crystallization state and nature of crystalline phases present within gels and powders were determined from X-ray diffraction analyses (XRD) using $\text{CuK}\alpha$ radiation (Phillips PW1820). The thermal decomposition of gels into powders was followed by thermogravimetry analyses (TGA, MTB 108). Grain morphology was obtained from scanning electronic microscope observations (SEM, JEOL 840). Particles were characterized in size according to the following vocabulary: crystallite and primary particle size. Crystallite size was determined from XRD measurements, which gives the average volume of perfectly coherent matter. It is calculated from Sherrer's formula:

$$D = \frac{0.9\lambda}{\sqrt{\beta_{\text{sample}}^2 - \beta_{\text{ref}}^2} \cos \theta} \quad [8]$$

where D is the crystallite size diameter (nm), $\lambda = 0.154$ nm, β the full-width at half-maximum (FWHM) of a diffraction peak at an angle θ and β_{ref} corresponds to the instrumental FWHM [8].

The primary particle size was determined from SEM observations using the classical "intercept method" [9]. It corresponds to what can be considered as the elementary particle of a ceramic powder and may consist of many crystallites. This characteristic dimension was rather small and some uncertainty may have occurred, in so far as the SEM resolution was limited for nanometric sizes.

3. Results and discussion

3.1. Gel characterization

3.1.1. Gel formation

Conditions of formation of gels strongly depended on the nature of the organic acid employed. In the case of tartaric and oxalic acids, white precipitates immediately appeared, while solutions remained limp for many hours in the case of other chelating agents. This difference in behavior remained after the gelification process (15 h at 115°C). Oxalic and tartaric gels were white and poorly viscous, while other samples were translucent and more viscous.

Chelating agent geometry may be argued to account for these different behaviors. In the case of tartaric and oxalic acids, double chelating "claw" geometry may initiate 1D or 2D polymeric structure formation [10,11], which is likely to quickly develop up to the formation of stable nucleus leading to the observed precipitation phenomena. In the case of malonic acid, only one chelating "claw" (forming a six-atom cycle) can act to develop an extended molecular structure and thus should not lead as easily to a precipitate. The other chelating functions of this acid involve only four-atom cycles and thus are not thermodynamically favored. In the same way, the lack of double opposite chelating "claw" for citric and acetic acids could account for the absence of a well-defined precipitation process.

Concerning gel viscosity, molecule geometry may, again, account for the previously observed behaviour differences. In the case of oxalic and tartaric acids, inter-chains or inter-plane bonds, such as Van der Waals bonds, can be formed during heat treatment at 115°C.

However, these bonds are weaker than intra-chains or plane bonds. Thus, mechanical strength of the resulting gel remains low and shear stress sensitive, which corresponds to a low viscosity. On the other hand, in the case of other chelating agents, formation of the gel takes place by solvent evaporation during heating. Building of a 3-D interconnected molecular edifice may occur when yttrium-chelated molecules are close enough to make hydrogen bonds after reducing the solution volume. The hydrogen bonds very often take place in aqueous media, and more especially with alcohols or organic acids [12]. Such hydrogen bond bridging molecules can therefore explain the higher viscosity of the resulting material.

3.1.2. Gel composition

XRD analysis of the materials obtained after heating at 115°C (named as precursor gel) shows that they contained at least one crystallized phase (Figs. 3a–e and 4a–d), except for the citric acid route with [citric acid]/[Y]=20 ratio. The corresponding XRD (Fig. 4e) pattern only shows a characteristic amorphous bumped background.

In the case of the precursor gel obtained with a [citric acid]/[Y]=2 ratio, the only crystallized phase observed may be assigned to ammonium nitrate, which comes from the starting compounds. In fact, a bumped background can also be noticed (Fig. 3e) which reveals the presence of an amorphous material, like in the [citric acid]/[Y]=20 ratio sample. Formation of an amorphous material seems to be favored when citric acid is used as a chelating agent. Actually, citric acid is widely used in sol–gel processes to obtain amorphous polyatomic materials [13]. For the PECHINI method, polycondensation processes take place due to the presence of polyol

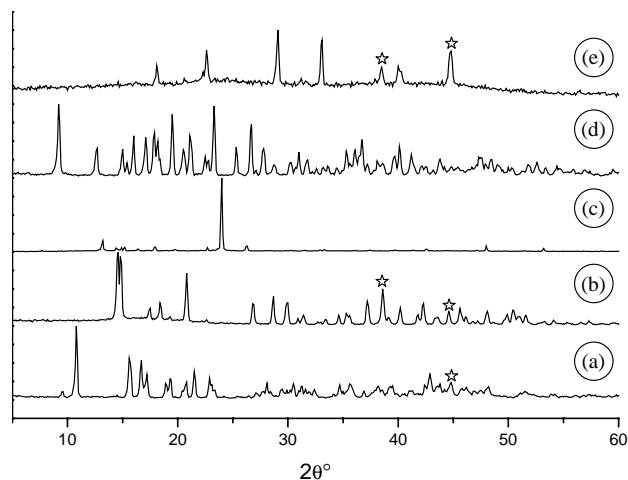


Fig. 3. XRD patterns of precursor gels before calcination, as a function of the chelating agent and for a [chelating agent]/[Y]=2 ratio: (a) acetic acid, (b) oxalic acid, (c) malonic acid, (d) tartaric acid and (e) citric acid.

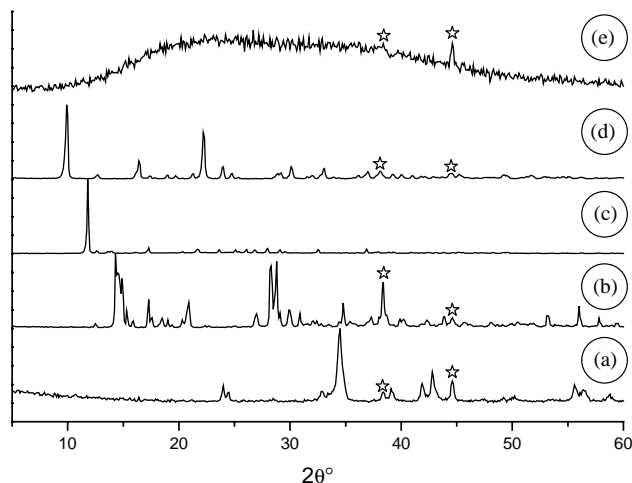


Fig. 4. XRD patterns of precursor gels before calcination, as a function of the chelating agent and for a [chelating agent]/[Y]=20 ratio: (a) acetic acid, (b) oxalic acid, (c) malonic acid, (d) tartaric acid and (e) citric acid.

molecules (usually ethylene glycol). For our experiment, gelification is related to solvent evaporation during the heating phase (115°C, 15 h). But, in both cases, the gelification process involves citric acid. Also, the amorphous character of the gel thus obtained may be explained by its peculiar non-planar molecule conformation and its seven possible chelating functions, which do not promote any long-range order during the growth of the gel at low temperatures.

For other chelating agents, it has not been possible to identify completely all crystallized phases present in precursor gels but it appeared clear that they resulted from the gelification process and that they involved yttrium. Obviously, it was checked that these phases could not be attributed to re-crystallization of initial compounds. The tartaric acid route is discussed here as an example. XRD patterns of starting tartaric acid powder, [tartaric acid]/[Y]=2 and 20 ratio precursor gels are presented in Fig. 5. As it can be seen, diffraction peaks of both precursor gels (Fig. 5c and d) do not correspond to the initial tartaric acid powder one. Moreover, none of these XRD patterns can be indexed according to JCPDS data file. Now, a blank gelification experiment was performed without yttrium and the XRD pattern of the material obtained is given in Fig. 5b. It reveals again the presence of crystallized phases, but these XRD peaks do not match those of the two precursor gels studied. It suggests then that the crystalline phases formed during gelification actually imply the yttrium cation.

As for the oxalic acid route, crystallized phases have been partly identified. The XRD pattern of the [oxalic acid]/[Y]=2 precursor gel (Fig. 3b) shows the exclusive presence of ammonium yttrium oxalate $\text{Y}(\text{NH}_4)(\text{C}_2\text{O}_4)_2 \cdot \text{H}_2\text{O}$ (JCPDS file no. 22-1047). The [oxalic

acid]/[Y]=20 gel precursor (Fig. 4b) also contains the same mixed salt and another non-referenced phase whose XRD pattern seems close to that of an hydrated yttrium oxalate (JCPDS file no. 40-1461); the differences may be attributed to the number of associated water molecules. In the same way, XRD pattern of [malonic acid]/[Y]=20 precursor gel (Fig. 4c) seems close to that of $Y_2(C_3H_4O_4)_3 \cdot 7H_2O$. For the [acetic acid]/[Y] route, no composition associating yttrium and acetate is reported in the JCPDS data file. However, SEM observation of the [acetic acid]/[Y]=20 precursor gel (Fig. 6) revealed needle-shaped grains within a matrix. EDS analyses performed on these needle-shaped grains, which should correspond to the crystallized phase (Fig. 4a), showed that they contained both yttrium and carbon.

In conclusion, all experimental observations suggest that yttrium, the chelating agent and their relative concentration play a key role in the gelification process

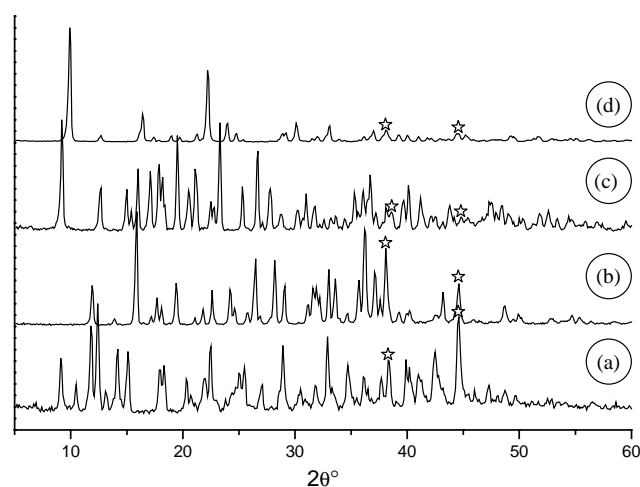


Fig. 5. XRD patterns of (a) initial DL-tartaric acid powder, (b) gel corresponding to the black gelification experiment (without yttrium), (c) precursor gel corresponding to [tartaric acid]/[Y]=2 ratio and (d) precursor gel corresponding to [tartaric acid]/[Y]=20 ratio.

that leads, excepted for the citric route, to the crystallized phase including yttrium. Most of these phases were not reported in the literature and may correspond to the partly dehydrated form of the yttrium chelate molecule.

3.1.3. Precursor gel morphology

Results concerning precursor gel morphologies are summarized in Table 1. No typical grain shape was observed for samples prepared from citric and malonic routes and for the [acetic acid]/[Y]=2 precursor gel. On the other hand, tartaric and oxalic acid routes lead to specific morphologies such as needles or platelets.

The gel-like morphology observed for the citric acid precursor gels agrees with its amorphous nature. On the other hand, malonic and acetic acid (ratio = 2) precursor gels show the presence of crystallized phases, even if no typical morphology is observed. But, as it was proposed for the gelification mechanism, the lack of double opposite chelating “claw” does not favor the development of precipitates and therefore of well-defined grains. This is confirmed by the large values of FWHM of XRD peaks, which indicate very little crystallite sizes for the crystalline phases belonging to these gels.

For tartaric and oxalic acid routes, grains present very specific shapes such as platelets or needles depending on the chelating agent or the concentration ratio (Fig. 8a2, b2, c2, d2). Similar results have been found concerning rare earth tartarate and oxalate [14,15]. Concerning the latter case, XRD measurements showed that the grains were related to yttrium oxalate phases. A platelet or needle-like crystallite growth can be understood in relation to the oxalic acid specific conformation made of two opposite chelating functions in the same plane. Crystallite development is expected in chain or plane, alternating yttrium and chelating molecule while chains or planes are connected together by weaker bonds. Tartaric acid possesses many possibilities to chelate yttrium but only two of them involve a six-atom cycle thermodynamically more stable than the other chelating cycles. These two chelation functions are in the

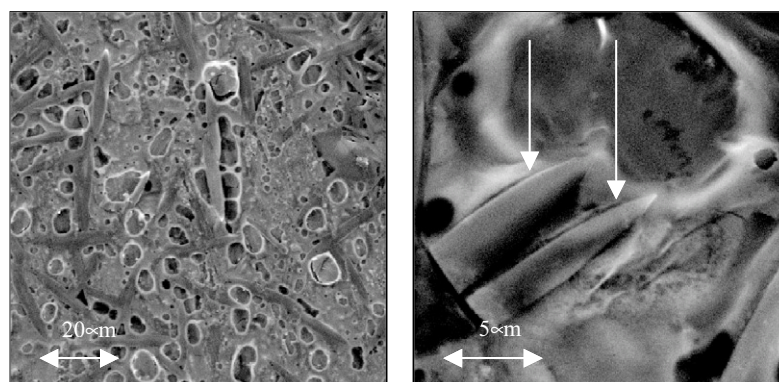


Fig. 6. SEM micrographs of precursor gel with acetic acid as chelating agent and with [acetic acid]/[Y]=20 ratio.

Table 1
Precursor gel morphologies (before calcination)

Sample	[Chelating agent]/[Y] ratio	
	2	20
Citric acid	Gel-like shape	Gel-like shape
Tartaric acid	Thin platelets	Needles
Malonic acid	Gel-like shape	Gel-like shape
Oxalic acid	Thick platelets	Platelets
Acetic acid	Gel-like shape	Needles included in a gel matrix

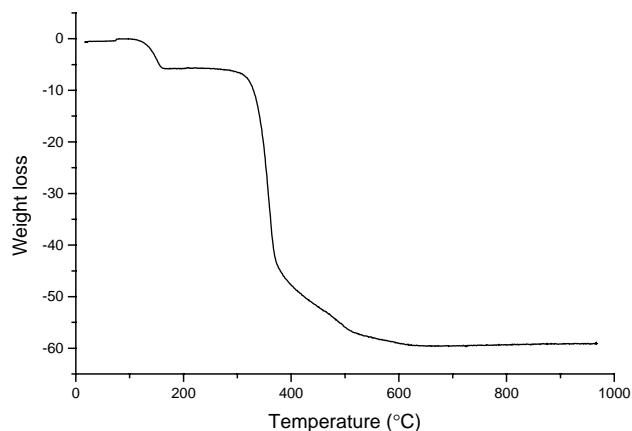


Fig. 7. TGA of precursor gel corresponding to [oxalic acid]/[Y]=2 ratio.

same planar geometry than oxalic acid, which is therefore likely to induce plate or chain-like growth, so that macroscopic shape looks like platelets or needles. Differences in morphology observed between gel precursors with [tartaric acid]/[Y]=2 and 20 ratios (Fig. 8b1 and c1) suggest that when tartaric acid concentration is in large excess, a complete 2D growth of particles is less favored than the needle shape which could be related to the easy formation of elongated grains during crystallization of pure tartaric acid.

3.2. Yttria powder characterization

3.2.1. Precursor gel decomposition

Thermal treatment of precursor gels gave rise in every case to Y_2O_3 powders at low temperatures. Of course, reactional processes leading to the oxide depended on the composition of the precursor gel.

Two particular cases can be mentioned: [malonic acid]/[Y]=2 and [acetic acid]/[Y]=20 gel precursors. For these two samples, a spontaneous auto-combustion reaction took place at 270°C and 340°C, respectively. This auto-ignition process may be attributed to a redox reaction between organic compounds acting as a reductant agent and the nitrate ions acting as oxidizing species [16]. For these specific compositions and

concentrations, exothermicity of the reaction is efficient enough to initiate an auto-ignition process like self-heating syntheses (SHS processes), leading to foamy and porous yttria powders.

Concerning all other samples, decomposition process occurred in many steps, that can be roughly separated in two domains below and above about 300°C. As an example, Fig. 7 shows the TGA curve of [oxalic acid]/[Y]=2 precursor gel. The first steps correspond to the transformation of the precursor gel to dehydrated ammonium yttrium oxalate, which then decomposes to give yttrium oxide between 300°C and 700°C. As a general rule, yttria was always formed at temperatures as low as 700°C, which allowed very fine particle size to be obtained.

3.2.2. Yttria powder XRD study

The yttria phase obtained after calcination treatment always presents the stable cubic structure. Lattice parameter was calculated ($a = 1.0604 \pm 0.001$ nm) and corresponds to the expected theoretical value ($a = 1.0604$ nm, JCPDS file no. 86–1326). Organic acid employed for the gelification process has no effect on the obtained yttria structure. The increase of the calcination temperature did not change the structural parameters, but led to a lowering of XRD peak width, which revealed crystallite size growth. Crystallite size was determined by the Sherrer's method for samples heat treated at 800°C and 1100°C. Primary particle sizes were also estimated from SEM observations. The results are summarized in Table 2. First, whatever the nature of the precursor gel was, the crystallite size remained almost the same for a given calcination temperature. Second, the average crystallite size increased, in all cases, from ~20 to 30 nm for 800°C calcined samples to ~40–70 nm for 1100°C calcined samples. Conversely, primary particle size does not seem to be affected by heating. In fact, these two types of measurements correspond to two different scales of characterization of particle size: lattice scale for the crystallite size and nanometric scale for primary particle size. Then, it means that Y_2O_3 particles that are formed after precursor gel decomposition are likely polycrystalline (made of many crystallites or containing many structural defects) and the calcination treatment allows mainly internal structural reorganization within the primary particles to be done (grain crystallization). Therefore, grain sizes remained in the nanometric range even after a 1100°C heat treatment. As a conclusion, whatever the conditions of preparation of gel precursor were, the calcined powders were structurally identical and gave very low particle size.

3.2.3. Yttria powder morphology

SEM micrographs of yttria powders are presented in Fig. 8. Grain morphologies are summarized in Table 3.

Table 2

Crystallite and primary particle sizes of yttria powders as a function of initial chelating agent and calcination temperature

Sample	$T_{\text{calcination}} = 800^{\circ}\text{C}$		$T_{\text{calcination}} = 1100^{\circ}\text{C}$	
	Crystallite size (nm)	Primary particle size (nm)	Crystallite size (nm)	Primary particle size (nm)
[Citric acid]/[Y]=2	21	60–100	35	No measurable grains
[Citric acid]/[Y]=20	Amorphous material	70–110	43	80
[Tartaric acid]/[Y]=2	33	220	60	90–170
[Tartaric acid]/[Y]=20	34	160	73	130–330
[Malonic acid]/[Y]=2	24	70–140	60	100–150
[Malonic acid]/[Y]=20	27	No measurable grains	55	No measurable grains
[Oxalic acid]/[Y]=2	36	No measurable grains	70	No measurable grains
[Oxalic acid]/[Y]=20	22	75–125	59	110
[Acetic acid]/[Y]=2	24	No measurable grains	37	100–200
[Acetic acid]/[Y]=20	31	100–200	55	100–200

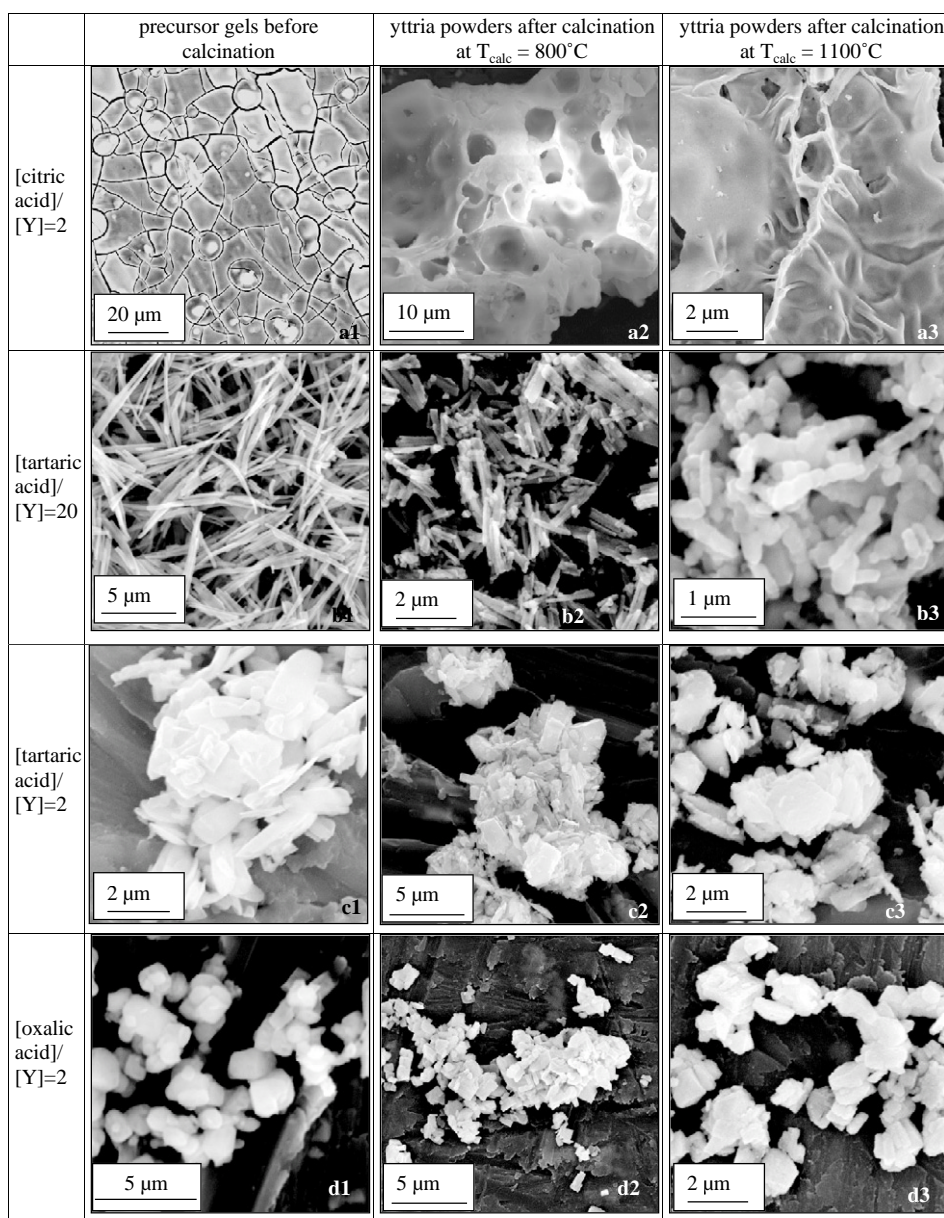


Fig. 8. SEM micrographs of precursor gels and yttria powders. (a) [citric acid]/[Y]=2, (b) [tartaric acid]/[Y]=20, (c) [tartaric acid]/[Y]=2, (d) [oxalic acid]/[Y]=2. (a1), (b1), (c1) and (d1): precursor gels before calcination; (a2), (b2), (c2) and (d2): yttria powders after calcination and $T_{\text{calc}} = 800^{\circ}\text{C}$; (a3), (b3), (c3) and (d3): yttria powders after calcination and $T_{\text{calc}} = 1100^{\circ}\text{C}$.

Table 3
Yttria powder morphologies as a function of the calcination treatment

Sample	Yttria powder morphologies at 800°C	Yttria powder morphologies at 1100°C
[Citric acid]/[Y] = 2	Sponge	Sponge
[Citric acid]/[Y] = 20	No typical morphology	Sponge
[Tartaric acid]/[Y] = 2	Sand stone shape	Sand stone shape
[Tartaric acid]/[Y] = 20	Needles	Grooved needles
[Malonic acid]/[Y] = 2	Sponge	Spherical grains
[Malonic acid]/[Y] = 20	Thin platelets	Thin platelets
[Oxalic acid]/[Y] = 2	Thick platelets	Thick platelets
[Oxalic acid]/[Y] = 20	Platelets	Platelets
[Acetic acid]/[Y] = 2	Thin platelets	Thin platelets
[Acetic acid]/[Y] = 20	No typical morphology	No typical morphology

Indeed, quite different yttria powder morphologies were obtained. The nature (Fig. 8a2, c2 and d2) and the relative concentration of organic acid used as chelating agent (Fig. 8b2 and c2) play a key role on the shape of these grains. Moreover, a very strong relationship can be noticed between precursor gel and yttria grain morphologies. Needles, platelets or absence of definite shape for a given precursor gel (Fig. 8a1, b1, c1 and d1) actually lead to the same grain shapes for the corresponding yttria powder (Fig. 8), even after a 1100°C heat treatment. Keeping the grain shape during the transformation from organic-rich precursors to oxide is quite a rare phenomenon since large chemical and structural rearrangements take place during decomposition. However, this so-called topochemical reaction has already been observed on doped oxysulfide compounds [17] and also on powders obtained by a sol-gel process when the high-temperature topology is close to the gel one [18]. Now, some other interesting features arise from these SEM observations. It appears that for some samples, grains obtained at 800°C break up into finer grains when heated at 1100°C. This is illustrated in Fig. 9 for the needles obtained through tartaric acid, for the acetic acid route where platelets broke into smaller pieces and for the malonic acid route where the foam collapsed into nanometric spherical grains. Such behaviors could seem inconsistent with classical grain growth phenomena related to a temperature increase. In fact, morphological evolution of such grain systems can be predicted quite precisely considering very simple thermodynamic analysis. Minimization of free energy of a polycrystalline granular system corresponds to a balance between variations of surface energy ($E_{\text{surf}} = \gamma_{\text{sg}} A_{\text{sg}}$ where γ_{sg} is the solid-gas surface tension and A_{sg} the solid-gas surface area) and variations of interface energy ($E_{\text{interf}} = \gamma_{\text{ss}} A_{\text{ss}}$ where γ_{ss} is the solid-solid surface tension and A_{ss} the solid-solid surface area). It has been already shown that polycrystalline fibers or films can break apart, depending on $\gamma_{\text{ss}}/\gamma_{\text{sg}}$ ratio and on geometrical characteristics of the system (grain size to fiber diameter or film thickness) [19–21]. In our

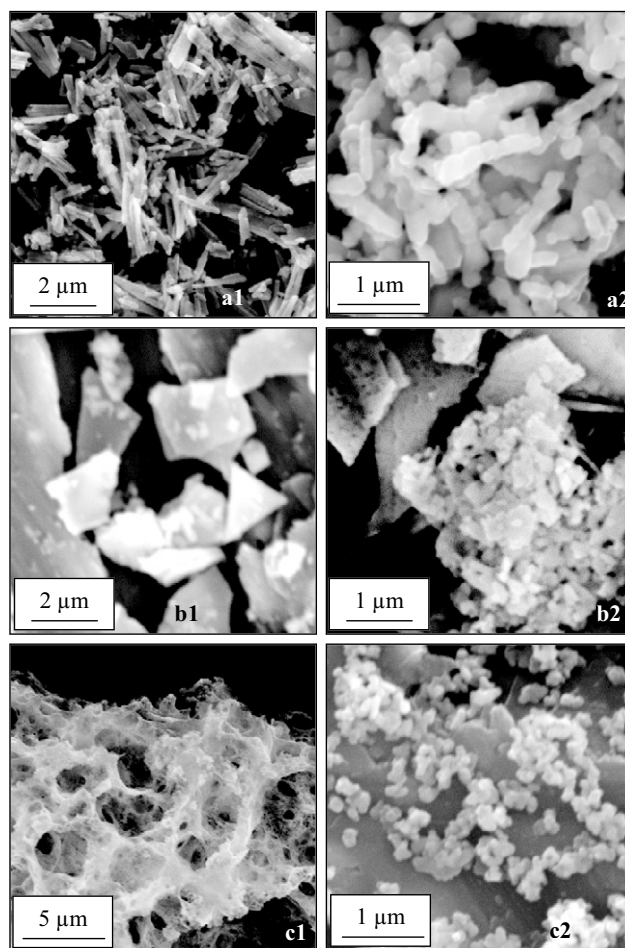


Fig. 9. SEM micrographs of yttria powders: (a1) [tartaric acid]/[Y] = 20 and $T_{\text{calc}} = 800^\circ\text{C}$, (a2) [tartaric acid]/[Y] = 20 and $T_{\text{calc}} = 1100^\circ\text{C}$, (b1) [acetic acid]/[Y] = 2 and $T_{\text{calc}} = 800^\circ\text{C}$, (b2) [acetic acid]/[Y] = 2 and $T_{\text{calc}} = 1100^\circ\text{C}$, (c1) [malonic acid]/[Y] = 2 and $T_{\text{calc}} = 800^\circ\text{C}$, (c2) [malonic acid]/[Y] = 2 and $T_{\text{calc}} = 1100^\circ\text{C}$.

experiments, crystallite size growth occurred during heat treatment from 800°C to 1100°C and when particle size reached the diameter of needles or the thickness of platelets, the breaking apart phenomenon could occur.

One can especially note that in the case of the malonic acid route, such a behavior leads to a non-agglomerated nanometric Y_2O_3 powder that looks very promising in terms of sinterability.

This study on grain shape evolution as a function of the nature of the used organic acid precursor and the temperature shows that, conversely to crystallographic characteristics, powder morphology is highly dependent on these parameters. These experiments can be considered as the first steps to improve control of morphology and grain size for yttria powders. It already shows that various shapes can be obtained and that spherical nanometric particles can be prepared at temperatures as high as 1100°C.

4. Conclusion

This work was aimed to propose new methods of preparation of very fine powders of Y_2O_3 suitable for sintering. A sol–gel process was defined, in which an organic acid that chelates yttrium, allows a gel to be formed after heating at 115°C. It has been shown that acetic, oxalic, malonic and tartaric acids led to the crystallization of grains constituted of yttrium chelate species, while the citric acid route mainly gave an amorphous material. Heat treatment of the precursor gels always gave Y_2O_3 powders above 700°C. The chelating agent composition did neither affect yttria composition nor structure. Crystallite size increased moderately during calcination of yttria powder, from about 30 nm at 800°C to 60 nm at 1100°C. On the other hand, chelating agent has a strong effect on yttria grain morphologies that are derivated closely from the morphology of precursor gel. This method could be used to prepare yttria powders with specific shapes such as fine needles or platelets. Moreover, in the case of malonic acid route, a nanometric, non-agglomerated powder was obtained which fulfilled the requirements needed for a good sintering.

Acknowledgments

This work was sponsored by the Commissariat à l’Energie Atomique and the authors also wish to express their gratitude to Region Aquitaine for its financial support.

References

- [1] J. Li, T. Ikegami, J. Lee, T. Mori, Y. Yajima, *J. Eur. Ceram. Soc.* 20 (2000) 2395–2405.
- [2] T. Ikegami, T. Mori, Y. Yajima, S. Takenouchi, T. Misawa, Y. Moriyoshi, *J. Ceram. Soc. Japan* 107 (1999) 297–299.
- [3] N. Saito, S. Matsuda, T. Ikegami, *J. Am. Ceram. Soc.* 81 (1998) 2023–2028.
- [4] Y.D. Jiang, Z.L. Wang, F. Zhang, H.G. Paris, C.J. Summers, *J. Mater. Res.* 13 (1998) 2950–2955.
- [5] P.L. Chen, I.-W. Chen, *J. Am. Ceram. Soc.* 79 (1996) 3129–3141.
- [6] D. Sordelet, M. Akinc, *J. Coll. Interf. Sci.* 122 (1988) 47–59.
- [7] Micheli, International Conference on Cer. Powd. Proc. Sci., Orlando, FL, USA, 1–4 November 1998.
- [8] H.P. Klug, L.E. Alexander, *X-Ray Diffraction Procedures*, Wiley, New York, 1954.
- [9] Am. Soc. Test. Mat. Annual book of ASTM Standards, Vol. 03.01, Philadelphia, PA, 1992, pp. 294–319.
- [10] E. Hansson, *Acta Chem. Scand.* 24 (8) (1970) 2969–2982.
- [11] W. Ollendorf, F. Weigel, *Inorg. Nucl. Chem. Lett.* 5 (1969) 263–269.
- [12] A. Durupthy, A. Casalot, A. Jaubert, *Chimie organique*, Hachette, Paris, 1996.
- [13] P.A. Lessing, *Ceram. Bull.* 68(5) (1989) 1002–1007.
- [14] T.R.R. Mac Donald, J.M. Spink, *Acta Crystallogr.* 23 (1967) 944–951.
- [15] P. Pascal, *Nouveau traité de chimie minérale*, Masson, Paris, 1959, pp. 1003–1024.
- [16] L. Fraigi, D.G. Lamas, N.E. Walsøe de Reça, *Nanostruct. Mater.* 11 (1999) 311–318.
- [17] J.M. Luiz, E.B. Stucchi, N. Barelli, *Eur. J. Solid State Inorg. Chem.* 33 (1996) 321–329.
- [18] A.C. Pierre, *Introduction aux procédés sol–gel*, Septima, Paris, 1992, p. 138.
- [19] K.T. Miller, F.F. Lange, *Acta Metallogr.* 37 (1989) 1343–1347.
- [20] K.T. Miller, F.F. Lange, D.B. Marshall, *J. Mater. Res.* 5 (1990) 151–160.
- [21] J.M. Heintz, J.C. Bihl, J.F. Silvain, *J. Eur. Ceram. Soc.* 19 (1999) 1759–1767.